

PCCP

Accepted Manuscript



This article can be cited before page numbers have been issued, to do this please use: S. Xing, P. Lv, J. Wang, J. Fu, P. Fan, L. Yang, G. Yang, Z. Yuan and Y. Chen, *Phys. Chem. Chem. Phys.*, 2016, DOI: 10.1039/C6CP06327F.



This is an Accepted Manuscript, which has been through the Royal Society of Chemistry peer review process and has been accepted for publication.

Accepted Manuscripts are published online shortly after acceptance, before technical editing, formatting and proof reading. Using this free service, authors can make their results available to the community, in citable form, before we publish the edited article. We will replace this Accepted Manuscript with the edited and formatted Advance Article as soon as it is available.

You can find more information about Accepted Manuscripts in the [author guidelines](#).

Please note that technical editing may introduce minor changes to the text and/or graphics, which may alter content. The journal's standard [Terms & Conditions](#) and the ethical guidelines, outlined in our [author and reviewer resource centre](#), still apply. In no event shall the Royal Society of Chemistry be held responsible for any errors or omissions in this Accepted Manuscript or any consequences arising from the use of any information it contains.

One-step hydroprocessing of fatty acids into renewable aromatic hydrocarbons over Ni/HZSM-5: Insight into the major reaction pathways

Shiyu Xing^{a,b,c,d}, Pengmei Lv^{a,b,d,e*}, Jiayan Wang^{a,f}, Junying Fu^{a,b,d}, Pei Fan^{a,b,c,d}, Lingmei Yang^{a,b,d}, Gaixiu Yang^{a,b,d}, Zhenhong Yuan^{a,b,d,e*}, Yong Chen^{a,b,d}

^aGuangzhou Institute of Energy Conversion, Chinese Academy of Sciences, Guangzhou 510640, China.

^bKey Laboratory of Renewable Energy, Chinese Academy of Sciences, Guangzhou 510640, China.

^cUniversity of Chinese Academy of Sciences, Beijing 100049, China.

^dGuangdong Key Laboratory of New and Renewable Energy Research and Development, Guangzhou 510640, China.

^eCollaborative Innovation Center of Biomass Energy, Henan Province, Zhengzhou 450002, China.

^fNano Science and Technology Institute, University of Science & Technology of China, Suzhou 215123, China.

*Corresponding author.

E-mail address: lvpm@ms.giec.ac.cn (P. M. Lv), yuanzh@ms.giec.ac.cn (Z. H. Yuan).

Abstract. For high calorificity and stability in bio-aviation fuels, a certain content of aromatic hydrocarbons (AHCs, 8–25 wt%) is crucial. Fatty acids, obtained from waste or inedible oils, are a renewable and economic feedstock for AHC production. Considerable amounts of AHCs, up to 64.61 wt%, were produced through the one-step hydroprocessing of fatty acids over Ni/HZSM-5 catalysts. Hydrogenation, hydrocracking, and aromatization constituted the principal AHC formation processes. At a lower temperature, fatty acids were first hydrosaturated and then hydrodeoxygenated at metal sites to form long-chain hydrocarbons. Alternatively, the unsaturated fatty acids could be directly deoxygenated at acid sites without first being saturated. The long-chain hydrocarbons were cracked into gases such as ethane, propane, and C₆–C₈ olefins over the catalysts' Brønsted acid sites; these underwent Diels-Alder reactions on the catalysts' Lewis acid sites to form the AHCs. The C₆–C₈ olefins were determined as critical intermediates for AHC formation. As the Ni content in the catalyst increased, the Brønsted-acid site density was reduced due to coverage by the metal nanoparticles. Good performance was achieved with a loading of 10 wt% Ni, where the Ni nanoparticles exhibited a polyhedral morphology which exposed more active sites for aromatization.

30 1 Introduction

31 The rapid, steady consumption of commercial transportation fuels such as aviation fuel,
32 commonly produced by petroleum refining ¹, has placed substantial burdens on the natural
33 environment through the excessive emission of greenhouse gases. The development of aviation
34 fuels derived from renewable and sustainable feedstocks has shown great potential because of
35 their ability to reduce the total carbon footprint by ~80% over their full life-cycle ², and has
36 attracted increasing interest in recent years ^{3,4}. Specifically designed for use in aircraft, aviation
37 fuels must meet stringent specifications such as high calorificity and low boiling points for safe,
38 high-altitude flight. Aromatic hydrocarbons (AHCs) are indispensable components of aviation
39 fuels because of their higher densities and volumetric heating values, in contrast to straight-chain
40 and iso-alkanes. More importantly, the presence of AHCs is necessary to ensure the shrinkage of
41 aged elastomer seals and prevent the leakage of aviation fuels ⁵. Therefore, for safe application,
42 current aviation fuels must contain 8–25% AHCs.

43 Because of their plentiful supply, ready accessibility, and low cost, biomass-derived feedstocks
44 for AHC synthesis are primarily composed of raw lignocellulosic materials such as cellulose,
45 hemicellulose, and lignin, and lipidic materials such as lipids and fatty acids ⁶⁻⁹. Several
46 researchers have investigated the synthesis of AHCs from biomass derivatives such as furans (e.g.,
47 2,5-dimethylfuran (DMF) or 2-methylfuran (MF)) and ethylene or propylene via Diels-Alder
48 cycloadditions and subsequent dehydration reactions ¹⁰⁻¹⁴. For example, toluene, a typical AHC,
49 could be synthesized through two principal steps: the Diels-Alder cycloaddition between MF and
50 ethylene, and the dehydrogenation of the cyclic intermediate to produce toluene ¹⁵. Unfortunately,
51 several side reactions also occurred during the Diels-Alder cycloaddition of MF and ethylene,
52 which made it difficult to achieve a high AHC yield and selectivity ¹⁰. Similarly, *p*-xylene could be
53 successfully synthesized from DMF and ethylene ^{11, 16}. However, for the conversion of
54 lignocellulose into AHCs, several pretreatment steps are needed, including the hydrolysis of
55 hemicellulose to xylose; the dehydration of xylose to furfural; and the hydrodeoxygenation of
56 furfural to 2-methylfuran.

57 Compared to lignocellulosic biomass, fatty acids require less pretreatment. Lipidic feedstocks
58 are abundantly available in waste or inedible oils, and are significantly renewable and sustainable.
59 More importantly, fatty acids share structurally similar characteristics with petroleum substrates

60 and should undergo hydroprocessing without additional pretreatments. Many studies have
61 extensively addressed the hydroprocessing of waste oils or fatty acids into renewable fuel-like
62 hydrocarbons, but the products are mainly either isomerized C₈–C₁₆ alkanes, or diesel-like
63 hydrocarbons, such as long-chain C₁₇ and C₁₈ alkanes, rather than AHCs¹⁷⁻²⁰. In our group, other
64 researchers have conducted the study of hydro-converting fatty acid methyl esters into renewable
65 alkane fuels with considerable isomerized ratios in the presence of solvent hexane and the
66 conversion routines were investigated^{21, 22}. The main transformation routines included (i) the
67 hydrosaturation of unsaturated feedstocks, (ii) the hydrodeoxygenation of the saturated oils or
68 fatty acids into long-chain alkanes via dehydration, decarbonylation, and decarboxylation
69 reactions, and (iii) the partial hydrocracking and isomerization of long-chain alkanes into products
70 with the required carbon numbers and properties^{9, 23}. Due to the challenge of obtaining highly
71 isomerized products in the third step to improve low-temperature fluidity, a number of studies
72 have concentrated on tuning the fatty acid hydroconversion process by employing advanced
73 metal-supported acidic zeolite catalysts^{21, 23, 24}.

74 However, these synthesized alkanes have not been able to meet the application specifications
75 and must be blended with conventional aviation fuel²⁵ due to the absence of AHCs. Some recent
76 works have reported the production of AHCs in the hydroprocessing of waste oils and fatty acids.
77 Li T. et al.²⁶ investigated the hydroprocessing of waste oil into jet biofuel using three types of
78 zeolites (*meso*-Y, SAPO-34, and HY) loaded with nickel. Their results indicated that *meso*-Y
79 exhibited a high jet-range alkane selectivity of 53% and an AHC selectivity of 13.4% in the liquid
80 fuel products. Rabaev M. et al.²⁷ found that a certain level of polyunsaturated fatty acids is
81 required to produce relatively high aromatics contents. Despite having structural similarity with
82 petroleum-based substrates, the hydroprocessing of fatty acids is considered to be quite different
83 from current petroleum refinery methods. Conventional methods for AHC synthesis employ the
84 catalytic reforming of oxygen-free naphtha into AHC-enriched reformat. However, a new
85 catalytic reaction system is required for the hydroprocessing of these oxygenated lipidic
86 feedstocks, because more complex reactions (e.g., hydrodeoxygenation) are involved. By
87 inference, hydrodeoxygenation should play an important role throughout the whole transformation
88 process, but that conclusion remains unsubstantiated at present. Hence, it is of prime importance
89 to clarify the conversion routes and catalytic mechanisms for AHC formation during the

90 hydroprocessing of fatty acids.

91 In this work, under solvent-free conditions, we employed the Ni-impregnated HZSM-5 catalyst
92 for one-step hydroprocessing of fatty acids and successfully obtained considerable amounts of
93 AHCs. The main catalytic reaction pathways were analyzed in detail on the basis of detected
94 intermediates. The catalytic roles of the loaded Ni metal and catalyst acid sites were
95 well-determined combining the catalyst characterization through scanning electron microscopy
96 (SEM), transmission electron microscopy (TEM), and pyridine-adsorbed infrared spectroscopy
97 (Py-IR), etc. The overall catalytic conversion routes for AHC formation were proposed and
98 discussed. The advantage of this work was that it provided a new facile, effective approach for the
99 mass production of renewable AHCs. Further, the major reaction pathways for AHCs formation
100 were first proposed and the catalytic mechanisms were investigated into deep as well.

101 2 Materials and methods

102 2.1 Materials

103 The fatty acids feedstock was purchased from Tianjin Damao Chemical Reagent Factory, China,
104 and its specific composition is shown in Table 1. Nickel nitrate hexahydrate $[\text{Ni}(\text{NO}_3)_2 \cdot 6\text{H}_2\text{O}]$
105 (98%, Reagent Plus) was purchased from Tianjin Fuchen Chemical Factory. The HZSM-5
106 supports with Si/Al ratios of 25, 80, 120, 150, and 200 were obtained from Nankai Catalysts
107 Industry, China. Cyclohexane (AR) was purchased from Aladdin, China. All materials were used
108 as received.

109 Table 1. Feedstock composition

Fatty acid	Fatty acid structure	Formula	Composition (wt%)
Palmitic acid	C16:0	$\text{C}_{16}\text{H}_{32}\text{O}_2$	8.36
Stearic acid	C18:0	$\text{C}_{18}\text{H}_{36}\text{O}_2$	3.59
Oleic acid	C18:1	$\text{C}_{18}\text{H}_{34}\text{O}_2$	67.20
Linoleic acid	C18:2	$\text{C}_{18}\text{H}_{32}\text{O}_2$	13.67
Linolenic acid	C18:3	$\text{C}_{18}\text{H}_{30}\text{O}_2$	2.87
Eicosenoic acid	C20:1	$\text{C}_{20}\text{H}_{38}\text{O}_2$	4.31

110 2.2 Catalyst preparation and characterization

111 Ni/HZSM-5 catalysts with different wt% nickel contents (5 wt%, 10 wt%, 12.5 wt% and 15

112 wt%) were prepared by the impregnation of the HZSM-5 supports in aqueous solutions of
113 $\text{Ni}(\text{NO}_3)_2 \cdot 6\text{H}_2\text{O}$. The Si/Al ratios of used HZSM-5 were 25, 80, 120, 150 and 200. The mixture
114 was stirred at 150 rpm for 6 h at ambient temperature, dried at 110°C for 12 h, and calcined at a
115 rate of 10°C/min from ambient temperature to 550°C and maintained for 8 h. After reduction
116 under H_2 atmosphere at 500°C for 2 h, Ni/HZSM-5 was finally obtained. For comparison, a Ni
117 metal catalyst was prepared by the calcination of $\text{Ni}(\text{NO}_3)_2 \cdot 6\text{H}_2\text{O}$ followed by H_2 reduction under
118 similar conditions. XRD measurements were carried out using an X'Pert PRO MPD
119 diffractometer (PANalytical) operated at 40 kV and 40 mA with $\text{Cu K}\alpha$ ($\lambda = 0.15406$ nm) radiation.
120 SEM was performed on a Hitachi S-4800 instrument operated at 10 kV. Before the SEM
121 experiment, samples were placed under an E1010 ion-sputtering instrument to improve
122 conductivity. TEM studies were carried out on a Hitachi H-7560 electron microscope with an
123 accelerating voltage of 100 kV. An X-ray fluorescence spectrometer (XRF, model: AxiosmAX
124 Petro, PANalytical B.V.) was used to identify the Ni contents of the prepared catalysts. The type of
125 acid sites on the catalysts was determined by recording infrared spectra of the substrates after the
126 adsorption of pyridine (Py-IR) using a Nicolet 6700 spectrometer.

127 **2.3 Hydroprocessing of fatty acids and product analysis**

128 The one-step hydroprocessing of fatty acids was conducted in a high-pressure autoclave with a
129 volume of 150 mL as shown in Figure S1. About 10 g feedstock and 0.6 g catalyst were added into
130 the reactor. After charging and discharging with hydrogen (99.999%) several times to remove
131 oxygen, the reaction system was pressurized to 4MPa with hydrogen. The H_2 /oil mol ratio was
132 calculated as 7.13. After 8 h reaction at a designated temperature (280°C, 320°C, 340°C, 360°C, and
133 380°C) with agitator stirring speed of 200 rpm, the reactor was immediately removed and cooled
134 with ambient-temperature water. The reactor pressure during the hydroconversion process was
135 monitored with a paperless recorder (Model VX5304R, Hangzhou Pangu Ltd., China). Gaseous
136 products were collected into a gas sampling bag, and the liquid products were sampled after
137 filtration through a 0.22 μm organic nylon 66 membrane (Tianjing Jinteng Ltd., China).

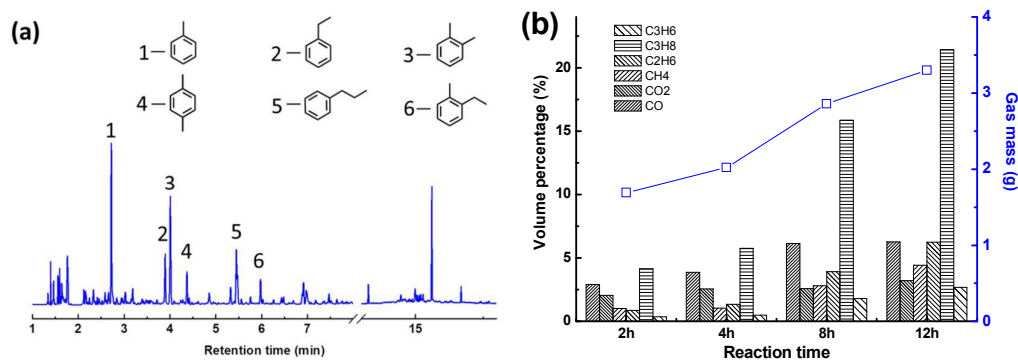
138 The gaseous products (CH_4 , CO , CO_2 , and $\text{C}_2\text{--C}_6$ hydrocarbons) were quantified with an
139 Agilent 7890A gas chromatograph (GC) equipped with a capillary column (GS-GASPRO, 60 m \times
140 0.32 mm), a thermal conductivity detector (TCD), and a flame-ionization detector (FID). The
141 composition of the liquid products was analyzed with a GC-mass spectrometry instrument

142 (GC/MS, Agilent 7890A-5975C) equipped with an Agilent HP-5MS column (5% phenyl methyl
143 silox, 30 m × 0.25 mm × 0.25 μm). Before being tested, the liquid products were diluted with
144 cyclohexane at a ratio of 1:100. The GC-MS test parameters were as follows. The diluted sample
145 (1 μL) was injected with a split ratio of 1:10 at 280°C. The initial column temperature of 60°C
146 was increased at 10°C/min to 300°C over 28.67 min. The major chemical constituents were
147 identified using the NIST 2014 Mass Spectral Library. The FID response was linear for each
148 component over the concentration ranges used, and the content analyses of the products generated
149 are summarized in terms of peak area %.

150 3 Results and discussion

151 3.1 Products distribution

152 The overall products distribution of the hydroprocessed fatty acids as a function of reaction time
153 is shown in Figure 1, and the yields of the produced AHCs are listed in Table 2. GC/MS analysis
154 of the liquid products shows that a large number of AHCs is produced, including toluene, *o*-xylene,
155 *p*-xylene, and propylbenzene (Figure 1(a)). Toluene, *o*-xylene, and 1-ethyl-2-methylbenzene are
156 the main AHC components. The total AHC content increases with reaction time, reaching 64.61
157 wt% after 12 h, as shown in Table 3. Other products such as alkanes, olefins, and cyclic
158 hydrocarbons are also formed, and their yields are shown in Table 3. After 2 h, the yields of
159 alkanes, olefins, cyclic hydrocarbons, and AHCs are 55.57, 7.48, 8.50, and 19.00 wt%,
160 respectively. With increasing reaction time, the alkane yield sharply decreases while that of the
161 AHCs greatly increases, suggesting that the AHCs are formed mainly from the transformation of
162 alkanes. Gases such as CO, CO₂, CH₄, C₂H₆, C₃H₈, and C₃H₆ are increasingly produced over time,
163 as illustrated in Figure 1(b), during the one-step hydroprocessing of the fatty acids.



164

165 Figure 1. GC spectra for liquid products (a) and gas products distributions (b). The compounds in

166 (a) were as follows: (1) toluene, (2) ethylbenzene, (3) *o*-xylene, (4) *p*-xylene, (5) propylbenzene,
167 (6) 1-ethyl-2-methyl-benzene. Reaction conditions: 360°C, 4 MPa H₂, 10 g fatty acids, 0.6 g 10 wt%
168 Ni/HZSM-5.

169 Table 2. AHC distribution as a function of reaction time (wt%)^a

AHC products	Toluene	Ethylbenzene	<i>o</i> -Xylene	<i>p</i> -Xylene	Propyl benzene	1-Ethyl-2-methylbenzene	Other ^b
2 h	6.53	2.20	5.12	0.75	0	3.09	1.31
4 h	9.90	3.07	7.10	0.77	0.87	4.31	4.63
8 h	15.61	4.51	12.17	2.84	1.48	7.50	9.85
12 h	16.87	5.38	13.81	2.59	1.47	9.18	15.31

170 ^aReaction conditions: 10 g fatty acids, 0.6 g 10 wt% Ni/HZSM-5, 360°C, 4 MPa H₂. ^bOther
171 products represent those containing one benzene ring and several methyl branches, as shown in
172 Figure S2.

173 Table 3. Liquid products distribution as a function of reaction time (wt%)^a

Products	Alkanes	Olefins	Cyclic hydrocarbons	AHCs	Fatty acids	Other ^b
2 h	57.57	7.48	6.50	19.00	5.16	6.55
4 h	39.94	14.98	5.21	30.65	1.26	4.30
8 h	28.18	7.33	5.06	53.96	0	0
12 h	14.07	4.33	4.59	64.61	0	0

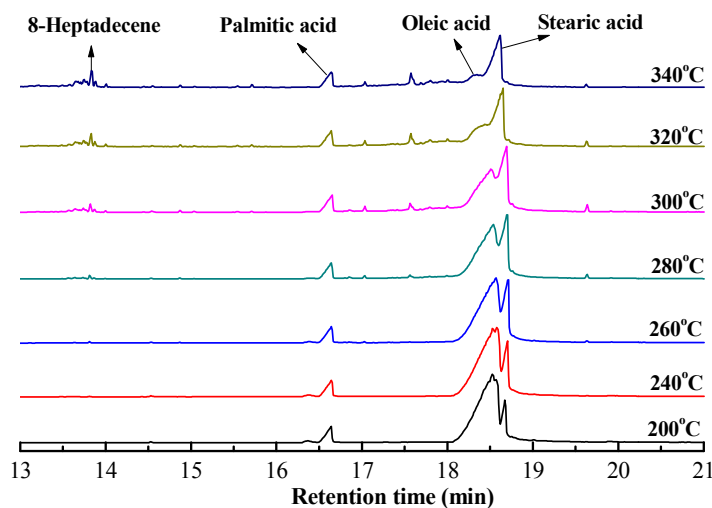
174 ^aReaction conditions: 10 g fatty acids, 0.6 g 10 wt% Ni/HZSM-5, 360°C, 4 MPa H₂. ^bOther
175 products represent oxygen-containing compounds such as octadecanol and octadecanal.

176 3.2 Major reaction pathways in the one-step hydroprocessing of fatty acids

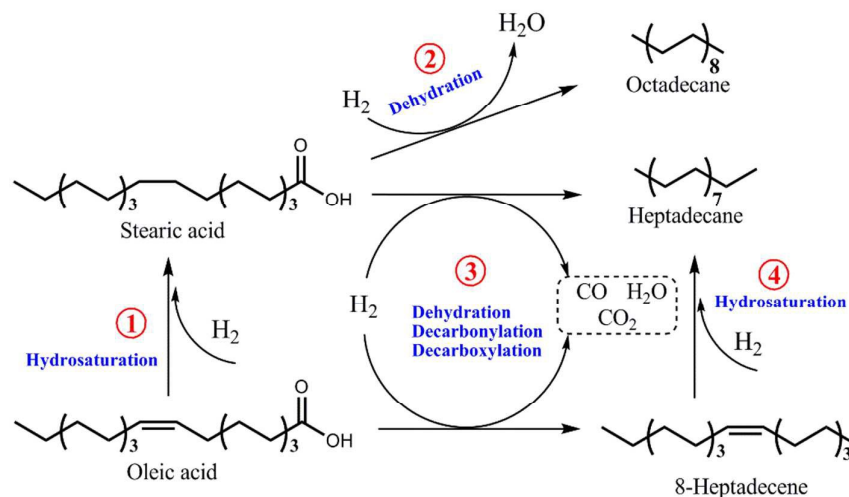
177 3.2.1 Hydrodeoxygenation

178 A variety of complex reactions, including hydrodeoxygenation, hydrocracking, and
179 aromatization, occur during the one-step hydroprocessing of fatty acids for AHC formation.
180 GC/MS spectra showing the intermediate product distributions during the heating period are
181 presented in Figure 2. Note that the fatty acids feedstock consists mostly of monounsaturated oleic
182 acid and polyunsaturated linoleic acid. Clearly, the yield of stearic acid increases as the reaction
183 temperature is elevated from 200 to 260°C. This reveals that unsaturated acids such as oleic acid

184 undergo hydrosaturation to form stearic acid, as shown by reaction ① in Figure 3. Jovanovic²⁸
 185 and Gabrovská²⁹ employed various nickel catalysts for the hydrogenation of unsaturated oils to
 186 produce vegetable tallow and fats in the temperature range of 145–190°C. They reported high
 187 selectivity in the hydrogenation of C18:3 (linolenic) into C18:2 (linoleic), C18:2 (linoleic) into
 188 C18:1 (oleic), and C18:1 (oleic) into C18:0 (stearic), respectively, but did not observe stearic acid
 189 as a major product. In this study, the further increase in the reaction temperature apparently
 190 promotes the hydrogenation of all the unsaturated C18 acids to stearic acid^{30,31}.



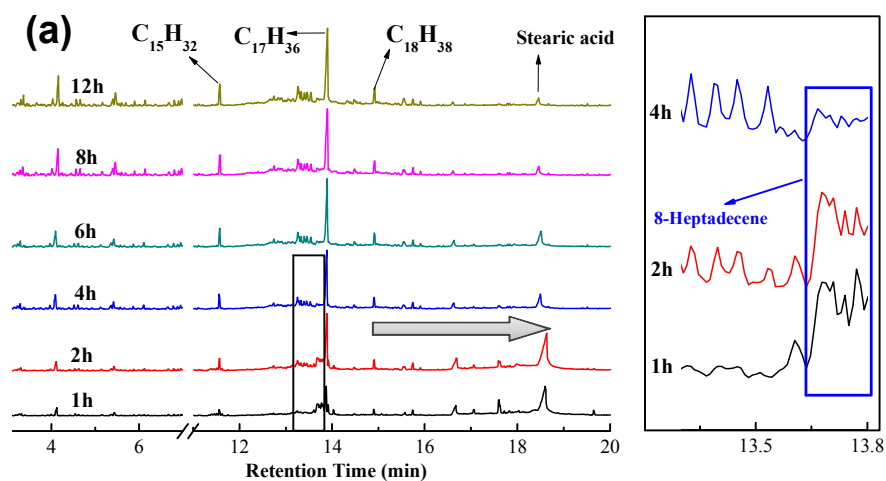
191
 192 Figure 2. GC/MS spectra obtained after heating at various temperatures. Reaction conditions: 10 g
 193 fatty acids, 0.6 g 10 wt% Ni/HZSM-5 (Si/Al = 25), 4 MPa H₂, 10°C/min heating rate.



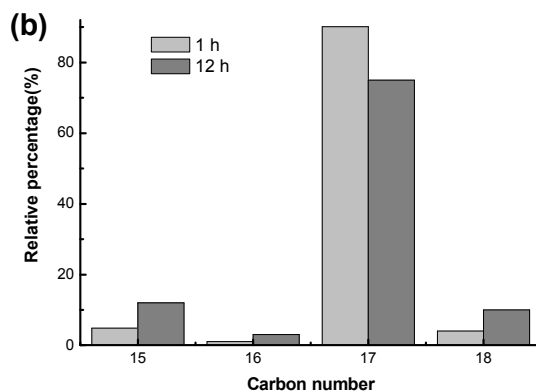
194
 195 Figure 3. Pathways for the hydrosaturation and hydrodeoxygenation of fatty acids, using oleic acid
 196 as an example and including reactions ①–④.

197 Subsequently, the saturated stearic acid is converted into long-chain hydrocarbons by

198 dehydration, decarbonylation, and decarboxylation reactions. Figure 4 shows the intermediate
 199 products distribution after the fatty acids are hydroprocessed for various reaction times at 320°C.
 200 Stearic acid is mostly transformed with increasing reaction time. Octadecane ($C_{18}H_{38}$) is found
 201 among the liquid products, suggesting the dehydration of stearic acid via reaction ② in Figure 3.
 202 The formation of heptadecane, CO, and CO_2 products (Figure 1(b)) indicates the dehydration,
 203 decarbonylation, and decarboxylation reactions of stearic acid, as depicted in reaction ③ of Figure
 204 3. Pentadecane ($C_{15}H_{34}$) is produced from palmitic acid via reaction ③. The partial enlargement of
 205 Figure 4(a) shows the presence of 8-heptadecene after 1 and 2 h reaction, suggesting that oleic
 206 acid can be directly deoxygenated without first being saturated, via reaction ③. After 4 h, the
 207 8-heptadecene is nearly completely consumed, most likely via hydrogenation to heptadecane
 208 (reaction ④). The relative percentages of C_{15} and C_{17} hydrocarbons after 1 h and 12 h reaction are
 209 both higher than those of C_{16} and C_{18} hydrocarbons, as shown in Figure 4(b), which suggested that
 210 the decarbonylation and decarboxylation reactions proceeded preferentially than the dehydration
 211 reaction during the whole process³².



212



213

214 Figure 4. (a) GC/MS spectra of fatty acid products after hydroprocessing for various reaction
215 times. (b) Relative percentages of C₁₅–C₁₈ hydrocarbons after 1 h and 12 h reaction. Reaction
216 conditions: 10 g fatty acids, 0.6 g 10 wt% Ni/HZSM-5 (Si/Al = 25), 320°C, 4 MPa H₂.

217 3.2.2 Hydrocracking

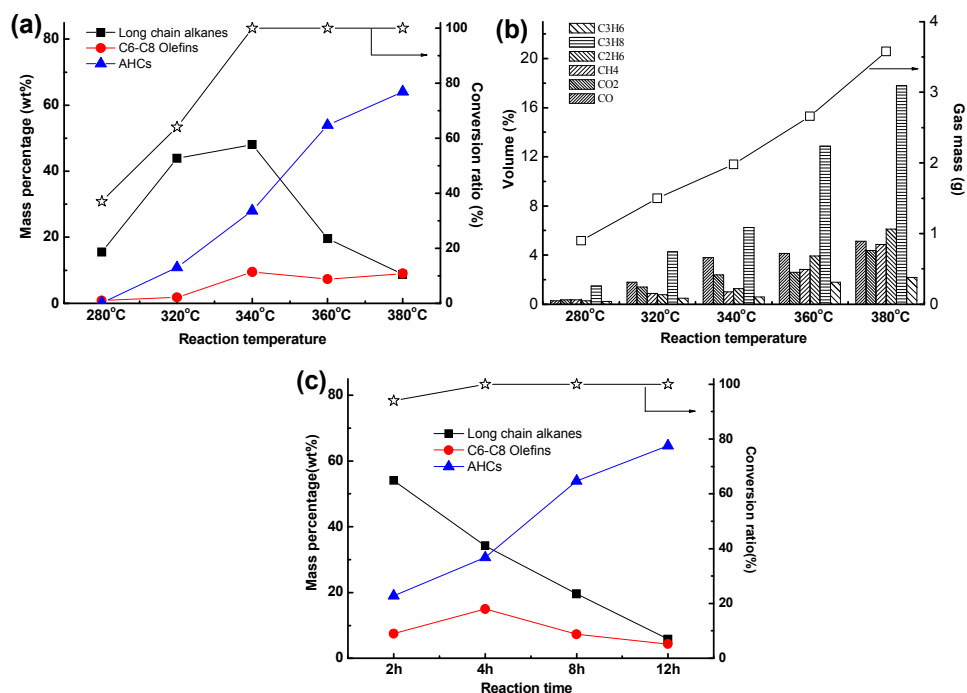
218 Long-chain hydrocarbons produced in the hydrodeoxygenation stage can be further cracked into
219 C₆–C₈ olefins and gases such as CH₄, C₂H₆, and C₃H₈ through a series of hydrocracking reactions.
220 Figure 5(a) shows the results after 8 h at temperatures of 280–380°C. The conversion ratio is
221 36.90 wt% at 280°C, and reaches 100 wt% at 340°C, demonstrating the significance of the
222 reaction temperature for the high conversion of fatty acids. The yield of alkanes is 15.90 wt% at
223 280°C, increases to a maximum value of 52.08 wt% at 340°C, and sharply drops to 25.18 wt% at
224 360°C. Although only minor amounts of olefins are produced at 320°C, this fraction increases to
225 9.5 wt% at 340°C and remains stable even at 380°C. The yields of cracked low-molecular-weight
226 gases increase at higher reaction temperatures, as shown in Figure 5(b). C₂H₆, and C₃H₈ are
227 mainly produced by thermal cracking and catalytic cracking processes³³⁻³⁵, respectively. However,
228 the yield of C₃H₈ is about three times higher than that of C₂H₆, suggesting that catalytic
229 hydrocracking is the main cracking process.

230 Figure 5(c) shows the hydroprocessing results with various reaction times at 360°C. The fatty
231 acids are mostly converted during the initial 2 h reaction period. At this stage, the alkanes yield is
232 the highest, up to 55.57 wt%, and the olefins yield is low (7.48 wt%). After 4 h, the yield of
233 alkanes decreases to 39.94 wt%, while the amount of olefins increases to 14.98 wt%. Details of
234 the alkane and short-chain olefin (C₆–C₈) structures are shown in Table 4. Straight-chain alkanes
235 with different carbon numbers are present in the liquid products, and a variety of C₆–C₈ olefins
236 such as 2-methyl-1-pentene, (Z)-3-methyl-2-pentene, and 2,4-dimethyl-1-pentene are produced.
237 Katikaneni and co-workers^{36, 37} conducted the catalytic conversion of canola oil over
238 potassium-impregnated HZSM-5, and obtained short-chain olefins. They believed that the
239 amorphous, non-shape-selective characteristics of the catalyst and severe thermal effects at
240 reaction temperatures of 400–500°C enhanced the subsequent secondary cracking of long-chain
241 hydrocarbons into lighter molecules.

242 For the alkane cracking process, two mechanisms have been previously proposed: a
243 monomolecular mechanism and a bimolecular mechanism. In the former, an acidic catalyst such

244 as a zeolite protonates an alkane to form a five-coordinate-carbon transition state^{38, 39}. This
 245 carbonium ion may undergo cracking to produce an alkane and an alkene, regenerating the catalyst
 246 by the loss of protons⁴⁰. The cracking products include dihydrogen, methane, and ethane. In the
 247 bimolecular mechanism, an alkane is activated by hydride transfer between the alkane and an
 248 adsorbed alkoxide species^{18, 41}. This reaction may be followed by β -scission or isomerization. Due
 249 to dimerization, oligomerization, isomerization, and β -scission reactions, the resulting product
 250 distribution is complicated. The sophisticated cracking products obtained in this study, which
 251 include methane, ethane, propane, and C₆–C₈ olefins, suggest that both these mechanisms are
 252 operative in the transformation of the long-chain alkanes. As the reaction time increases, the yields
 253 of long-chain alkanes decrease, indicating that hydrocracking reactions proceed concurrently.
 254 Moreover, the olefin yields also decrease after longer reaction times, suggesting that the produced
 255 C₆–C₈ olefins are not accumulated, but rather, are quickly converted.

256



257

258 Figure 5. Conversion ratios and yields of long-chain alkanes, C₆–C₈ olefins, and AHCs as a
 259 function of reaction temperature (a) and time (c). Gas yields at various reaction temperatures (b).

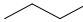
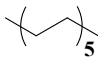
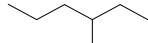
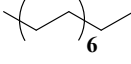

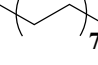
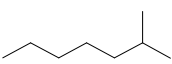
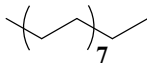
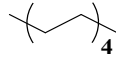
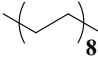
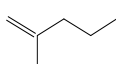
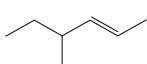
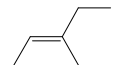
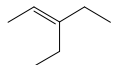
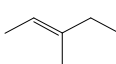
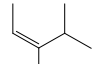
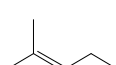
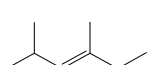
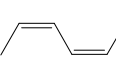
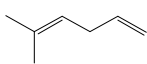
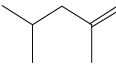
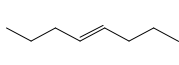
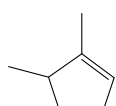
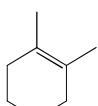
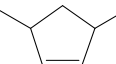
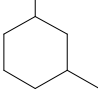
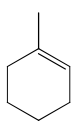
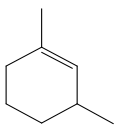
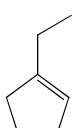
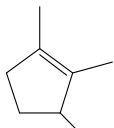
260 Reaction conditions: (a) and (b) 10 g fatty acids, 0.6 g 10 wt% Ni/HZSM-5 (Si/Al = 25), 4 MPa

261 H₂, 8 h, and (c) 10 g fatty acids, 0.6 g 10 wt% Ni/HZSM-5 (Si/Al = 25), 360°C, 4 MPa H₂.

262

263 Table 4. Structures of alkanes, short-chain olefins (C₆–C₈), and cyclic hydrocarbons after 4 h at

264 360°C

Retention time(min)	Compound name	Structure	Retention time(min)	Compound name	Structure
Alkanes					
1.34	Butane		9.19	Dodecane	
1.97	3-Methylhexane		13.26	Pentadecane	
2.1	Heptane		15.01	Hexadecane	
2.67	2-Methylheptane		15.61	Heptadecane	
4.42	Decane		16.70	Octadecane	
Short-chain olefins (C₆–C₈)					
1.62	2-Methyl-1-pentene		2.16	(E)-4-Methyl-2-hexene	
1.67	(Z)-3-Methyl-2-pentene		2.20	3-Ethyl-2-pentene	
1.72	3-Methyl-2-pentene		2.23	3,4-Dimethyl-(Z)-2-pentene	
1.77	2-Methyl-2-pentene		2.48	2,4-Dimethyl-3-hexene (c,t)	
1.87	(Z),(Z)-2,4-Hexadiene		2.58	5-Methyl-1,4-hexadiene	
2.03	2,4-Dimethyl-1-pentene		3.03	(E)-4-Octene	
Cyclic hydrocarbons					
2.12	1,5-Dimethylcyclopentene		2.54	1,2-Dimethylcyclohexene	
2.24	3,5-Dimethylcyclopentene		2.84	1,3-Dimethylcyclohexane	
2.30	1-Methylcyclohexene		3.06	1,3-Dimethyl-1-cyclohexene	
2.41	1-Ethylcyclopentene		3.19	1,2,3-Trimethylcyclopentene	

265

12

266 **3.2.3 Aromatization**

267 The produced C₆–C₈ olefins and small alkane molecules can cyclize and, by means of
268 aromatization, be converted into various types of AHCs. As shown in Figure 5(a), more AHCs are
269 produced at higher reaction temperatures, whereas the olefin yields remain stable at 9.5 wt%
270 without accumulation. Figure 5(c) shows a decreasing yield of the C₆–C₈ olefins with reaction
271 time, which suggests that these compounds are crucial intermediates for AHC formation. A variety
272 of cyclic hydrocarbons, amounting to ~5 wt%, were identified in the liquid product mixture, as
273 shown in Table 4. The cyclic hydrocarbons are mainly five- and six-membered ring compounds
274 such as 1,5-dimethylcyclopentene and 1-methylcyclohexene, respectively.

275 At a rather high temperature (380°C), substantial changes in the reaction pressure are observed
276 (see Figure S3). The distributions of the gaseous products CH₄, C₂H₆, and C₃H₈ obtained from
277 alkane hydrocracking in this process are shown in Figure 6. The slope (*k*) of each line segment in
278 Figure 6 signifies the change in a product's formation rate. Higher *k* values in Table 5 indicate that
279 more alkanes are cracked into gases, and *vice versa*. For better comparison, it was assumed that
280 the increased yield of every type of produced gas was proportional to the decreased amount of the
281 total alkanes. To characterize the relative changes, parameter *n* (defined as the absolute value of
282 the ratio of *k* (produced gas) vs. *k* (alkanes)) was used to eliminate the effect of the decreasing
283 alkane content on the equilibrium of the cracking reactions. The lower *n* value (see Table 5) from
284 *n*₂₋₄ to *n*₄₋₈ for C₃H₈ signifies that C₃H₈ is consumed during the 4–8 h reaction time. In comparison,
285 the higher *n* values of CH₄ and C₂H₆ suggest that these products are generated via other routes in
286 addition to alkane hydrocracking. H₂ is consumed in the hydrodeoxygenation and alkane
287 hydrocracking processes. The *n* value for H₂ is lower during the 4–8 h reaction period compared
288 to 2–4 h, suggesting that there are additional sources of H₂ production in this process. Here, it is
289 considered that the consumed C₃H₈ is transformed to AHCs, and in this process, CH₄, C₂H₆, and
290 H₂ are produced simultaneously.

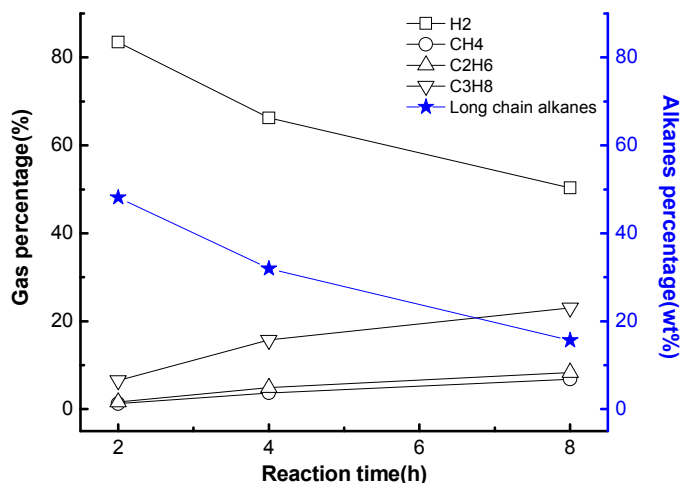


Figure 6. Gas and alkane percentages after different reaction times at 380°C.

291

292

293 Table 5. Changes in product formation rate over time.

k	Alkanes	CH ₄	C ₂ H ₆	C ₃ H ₈	H ₂
k_{2-4}^a	-8.09	1.23	1.65	4.60	-8.62
k_{4-8}^a	-4.08	0.78	0.86	1.82	-3.98
n_{2-4}^b	-	0.15	0.20	0.57	1.07
n_{4-8}^b	-	0.19	0.21	0.45	0.98

294 ^a k was the slope value of line segment 2-4 and 4-8295 ^b n was defined as the absolute value of the ratio of k (produced gas) vs. k (alkanes). For296 instance, $(n_{2-4})_{CH_4} = \left| \frac{(k_{2-4})_{CH_4}}{(k_{2-4})_{Alkanes}} \right| = \left| \frac{1.23}{-8.09} \right| = 0.15$.

297 In recent publications, aromatics were proposed to be formed by the Diels-Alder reactions of
 298 olefins^{10,42}. Depeyre et al.⁴³ examined the steam cracking of *n*-hexadecane at 750–850°C in a
 299 quartz flow reactor, with the aim of maximizing alkene production. They found that aromatics
 300 were increasingly formed at the expense of liquid olefin compounds with increasing temperature
 301 and reaction time. Cheng and Huber¹³ studied the co-feeding of olefins (ethylene and propene)
 302 with a series of furanoid compounds over a ZSM-5 catalyst. They found that co-feeding propene
 303 with furan (a C₄ diene) and 2-methylfuran (a C₅ diene), respectively, increased the selectivity for
 304 toluene and xylenes, which clearly suggested Diels-Alder cycloaddition reactions between the
 305 olefins and furans. Similar cases were also reported by Williams⁴⁴ and Nikbin¹⁴. Ethylene has
 306 also been frequently used as a substrate for aromatics production with biomass-derived furans¹¹.

307 As shown in Figure 6, many small alkanes such as ethane and propane are produced in this
308 process, and they can be directly dehydrogenated into ethylene and propene, respectively. In
309 addition, various types of C₆–C₈ olefins are produced. It is therefore suggested that Diels-Alder
310 reactions between these olefins can account for the produced AHCs.

311 Four pathways are presented in Figure 7 to illustrate the possible reactions involved in AHC
312 formation. First, a molecule of propane is dehydrogenated to propene, which can be combined
313 with a C₆ olefin such as 3-methyl-2-pentene to form a C₇ molecule with a five-membered ring.
314 Through ring expansion^{45,46}, the five-membered carbocycle is reformed to a six-membered ring.
315 Subsequently, after the removal of hydrogen, this is transformed into toluene, as shown in
316 pathway (1). In the second case, a six-membered hydrocarbon ring such as
317 1-ethyl-6-methylcyclohexene is directly formed through cyclization, as shown in pathway (2).
318 Dehydrogenation then affords 1-ethyl-6-methylbenzene. Alternatively, as shown in pathway (3),
319 the six-membered ring hydrocarbon, after demethanization, can be converted into
320 1,6-dimethylcyclohexene, which forms *o*-xylene after dehydrogenation. C₆–C₈ olefins such as
321 5-methyl-1,4-hexadiene, through self-cyclization⁴⁷, can form five- or six-membered ring
322 hydrocarbons, as shown in pathway (4). A small number of higher-molecular-weight AHCs⁴⁸ with
323 9 or more carbon atoms (e.g., 1,2,4-trimethylbenzene, 1-ethyl-2,4-dimethylbenzene, and
324 1-methyl-3-propylbenzene, as shown in the Figure S2) may be formed through direct cyclization
325 and dehydrogenation reactions between two C₆–C₈ olefins.

326

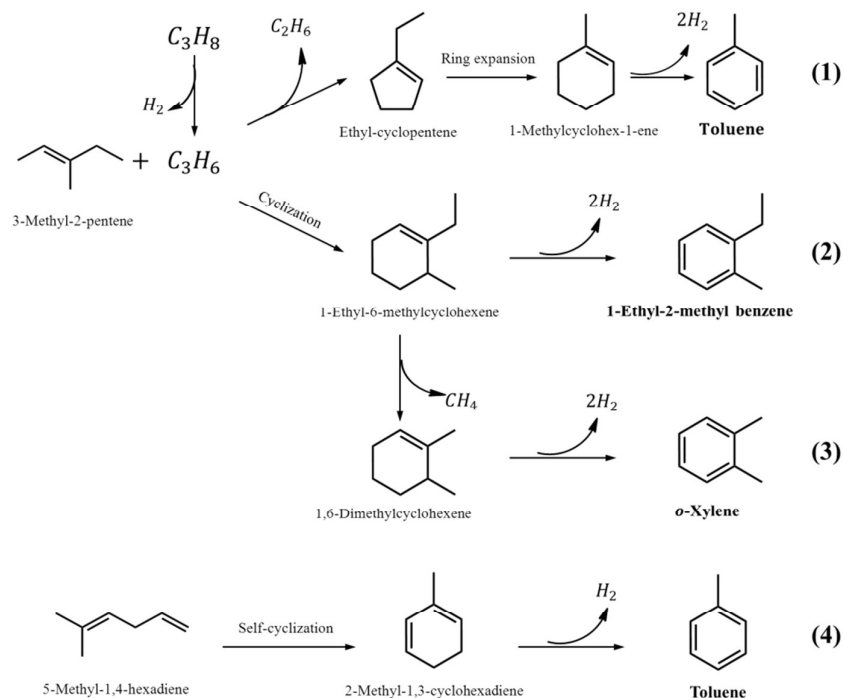


Figure 7. Possible pathways for AHC formation.

327

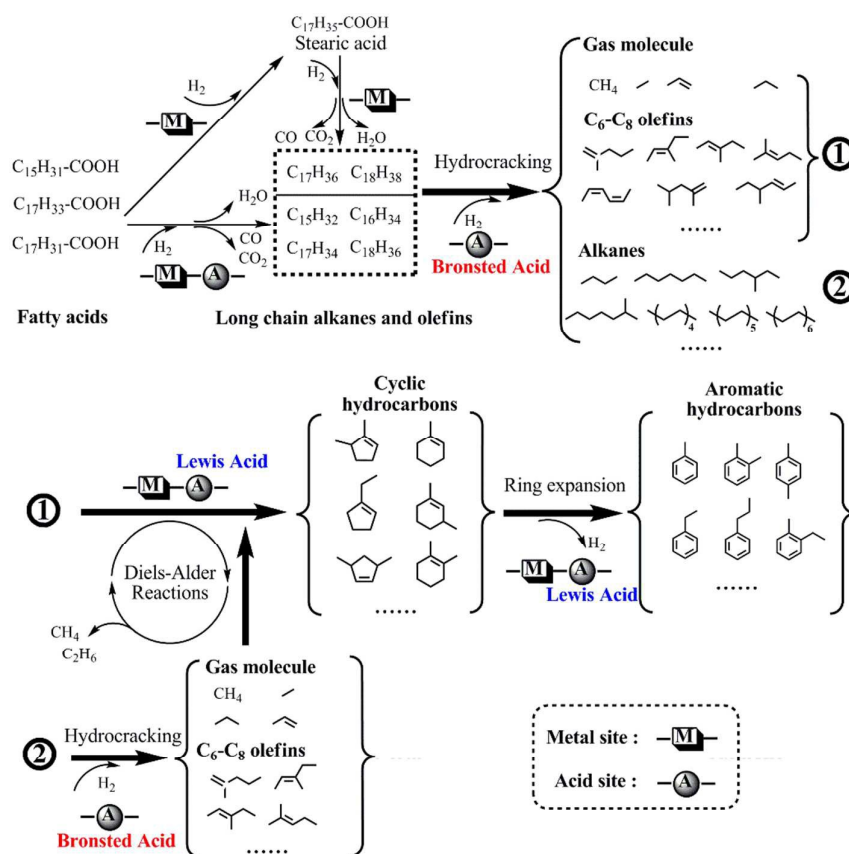
328

329 **3.3 Catalysis mechanisms**

330 According to the foregoing results, conversion routes for the one-step hydroprocessing of fatty
 331 acids are proposed in Figure 8; these mainly consist of hydrodeoxygenation^{19, 20, 31, 49, 50},
 332 hydrocracking, and aromatization processes. The first step is the hydrodeoxygenation of the fatty
 333 acids into long-chain hydrocarbons, including the hydrosaturation of oleic and linoleic acids into
 334 stearic acid at a low reaction temperature^{28, 29}. Subsequently, the long-chain hydrocarbon products
 335 are transformed into short-chain compounds by thermal and catalytic hydrocracking reactions.
 336 These cracking products include: the gases methane, ethane, and propane; abundant C_6 – C_8 olefins
 337 such as 2-methyl-1-pentene, (*Z*)-3-methyl-2-pentene, and (*Z*),(*Z*)-2,4-hexadiene (with two $C=C$
 338 bonds); a few types of short-chain alkanes such as butane, 3-methylhexane, and heptane; and
 339 long-chain alkanes, including pentadecane. After the C_6 – C_8 olefins and propene undergo
 340 Diels-Alder reactions, cyclic hydrocarbons with five- or six-membered rings containing $C=C$
 341 bond(s) are formed. The five-membered hydrocarbon rings can be converted into six-membered
 342 hydrocarbon rings through ring-expansion reactions. Eventually, these six-membered ring
 343 hydrocarbons are transformed into AHCs by dehydrogenation.

344 When pure Ni metal (see XRD patterns in Figure S4) was used as the catalyst for the one-step

345 hydroprocessing of the fatty acids, the vast majority of the products (~93 wt%) consisted of
 346 long-chain alkanes (Figure 9). Thus, Ni metal perfectly facilitates the hydrodeoxygenation
 347 reactions but has almost no effect on the hydrocracking of long-chain alkanes. In contrast, as little
 348 as 25.18 wt% alkanes remain when using the 10 wt% Ni/HZSM-5 catalyst, indicating the
 349 enhanced hydrocracking with HZSM-5. This zeolite has abundant nano-holes with size of 0.55 nm
 350 ²², which are much smaller than the size of the long-chain alkane molecules. This suggests that the
 351 surface properties of the catalyst are quite critical for the hydroconversion process, particularly the
 352 acid sites ⁵¹.



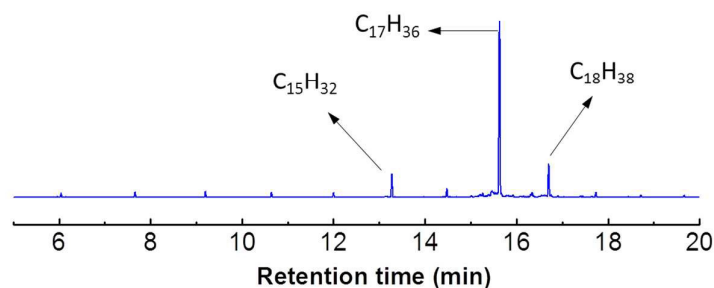
353

354 Figure 8. Proposed conversion routes for AHC formation in the one-step hydroprocessing of fatty

355

acids.

356



357

358 Figure 9. GC/MS spectra of products from the hydroprocessing of fatty acids using Ni metal

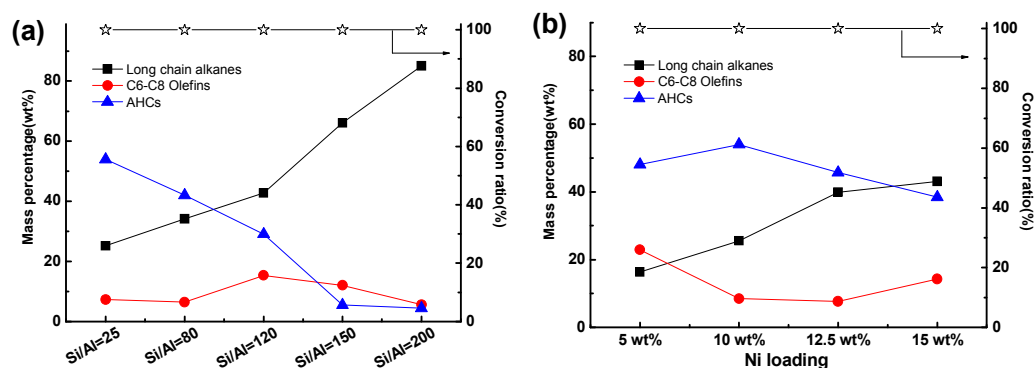
359 catalyst. Reaction conditions: 10 g fatty acids, 0.6 g Ni metal, 360°C, 4 MPa H₂, 8h.

360 The Si/Al ratios of the catalyst have a significant impact on the catalytic performance and the
361 product distribution. It is remarkable that, with increasing Si/Al ratios, the yield of long-chain
362 alkanes begins to increase and they become the major products, affording as much as 85.04 wt%
363 at Si/Al = 200 (Figure 10(a)). This suggests the inhibition of the hydrocracking of the long-chain
364 hydrocarbons. Note that the olefin yield increases to 15.36 wt% at Si/Al = 120 compared to Si/Al
365 = 80, but then decreases to 5.61 wt% at Si/Al = 200. It was reported that the cracking and
366 dehydrogenation of alkanes to form olefins take place at the Brønsted acid sites⁴⁸. The Py-IR
367 results in Table 6 show the highest density of Brønsted acid sites (0.12 mmol/g) for Si/Al = 25, but
368 this decreases sharply to 0.01 mmol/g at Si/Al = 200. Obviously, the decrease in the density of
369 Brønsted acid sites results in fewer long-chain alkanes being cracked. Moreover, the increase in
370 the recovery of C₆–C₈ olefins in the Si/Al range of 25–120 signifies the high cracking degree of
371 long-chain alkanes when the density of Brønsted acid sites exceeds 0.06 mmol/g. Thus, a high
372 number of Brønsted acid sites in the catalyst can effectively facilitate the hydrocracking of
373 long-chain alkanes.

374 According to previous investigations, the Diels-Alder reaction relies, to a great extent, on the
375 Lewis acidity of the catalyst⁵²⁻⁵⁴. Recently, it was shown that the Lewis-acidic catalyst plays a
376 significant role in the production of renewable aromatics by the tandem Diels-Alder cycloaddition
377 and dehydration reactions of biomass-derived dimethylfuran and ethylene^{12, 15, 55}. In those studies,
378 the high selectivity for toluene by the Lewis-acidic catalysts was mainly attributed to their ability
379 to accelerate the cycloaddition of dimethylfuran and ethylene and retard side reactions such as
380 oligomerization and alkylation. In the case of Brønsted-acidic zeolites, the side reactions were
381 significantly enhanced, resulting in lower selectivity for AHCs. As shown in Table 6, the highest

382 yield of AHCs, up to 53.96 wt%, is obtained at Si/Al = 25, at which the catalyst has a high Lewis
383 acid content of 0.06 mmol/g. However, the yield decreases quickly to 4.39 wt% at Si/Al = 200,
384 with only 0.02 mmol/g Lewis acid sites, suggesting the restriction of the Diels-Alder reactions
385 necessary for AHC formation.

386 It is noteworthy that the yield of C₆–C₈ olefins over catalysts with different Si/Al ratios is
387 determined by the degrees of both the hydrocracking of long-chain alkanes at the Brønsted acid
388 sites and the Diels-Alder reactions for AHC formation at the Lewis acid sites. For Si/Al = 25, the
389 low yield (25.18 wt%) of long-chain alkanes suggests a high degree of the hydrocracking reaction
390 on the Brønsted acid sites to produce C₆–C₈ olefins. However, the yield of C₆–C₈ olefins could be
391 as low as 7.33 wt%, which signifies that these olefins are ultimately transformed into AHCs on the
392 Lewis acid sites. When the catalyst Si/Al ratio is 120, the hydrocracking of the long-chain alkanes
393 still occurs to a significant extent due to the relatively adequate amount of Brønsted acid sites.
394 However, the insufficient number of Lewis acid sites inhibits the Diels-Alder reactions for AHC
395 formation, which leads to the increased yields of C₆–C₈ olefins. For Si/Al = 200, the high yield of
396 long-chain alkanes indicates a reduction in the extent of hydrocracking, which directly leads to
397 decreased yields of both the C₆–C₈ olefins and AHCs. It can be thus concluded that the Brønsted
398 and Lewis acid sites of the catalyst both influence the formation of AHCs.



399
400 Figure 10. Conversion ratios and productions of alkanes, C₆–C₈ olefins, and AHC products for
401 various Si/Al ratios and different Ni loadings. Reaction conditions: (a) 10 g fatty acids, 0.6 g 10 wt%
402 Ni/HZSM-5, 4 MPa H₂, 8 h, 360°C and (b) 10 g fatty acids, 0.6 g Ni/HZSM-5 (Si/Al = 25), 360°C,
403 4 MPa H₂, 8 h.

404

405

406 Table 6. Acid site densities of the prepared catalysts with different Si/Al ratios, determined by
407 Py-IR

Si/Al ratio	Ni content (wt%)	Acid site contents (mmol/g)			AHC yield (wt%)
		Brønsted	Lewis	Total	
25	10 (9.89) ^a	0.12	0.06	0.18	53.96
80	10 (9.91) ^a	0.08	0.04	0.12	41.99
120	10 (9.94) ^a	0.06	0.03	0.09	29.05
150	10 (9.90) ^a	0.03	0.03	0.06	5.47
200	10 (9.96) ^a	0.01	0.02	0.03	4.39

408 ^aActual Ni loading content (in the bracket) determined by XRF.

409 Table 7. Acid site densities of the prepared catalysts with different Ni contents, determined by
410 Py-IR

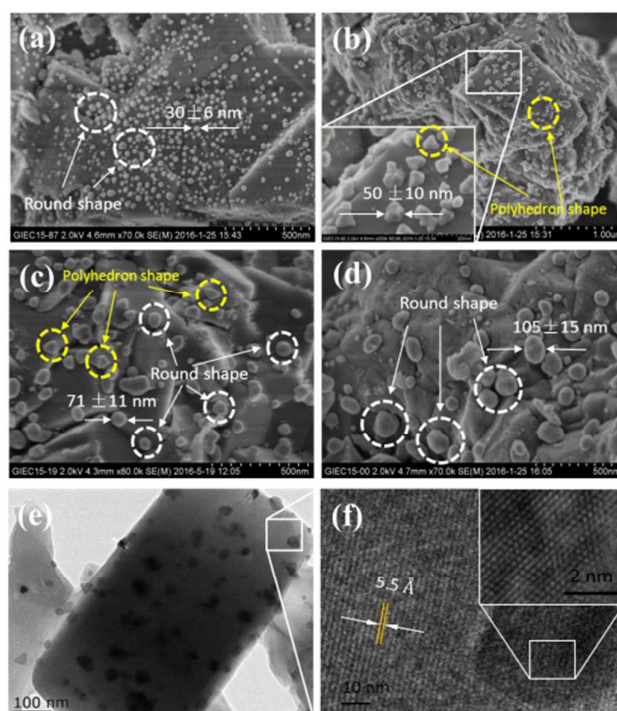
Si/Al ratio	Ni content (wt%)	Acid site contents (mmol/g)			AHC yield (wt%)
		Brønsted	Lewis	Total	
25	5 (4.92) ^a	0.14	0.08	0.24	48.09
25	10 (9.91) ^a	0.12	0.06	0.18	53.96
25	12.5 (12.43) ^a	0.11	0.06	0.17	45.73
25	15 (14.95) ^a	0.10	0.06	0.16	38.43
-	100 ^b	0	0.005	0.005	0

411 ^aActual Ni loading content (in the bracket) determined by XRF. ^bNi metal catalyst without
412 HZSM-5.

413 As mentioned above, pure Ni metal has almost no acid sites. We attempted to tune the catalyst
414 acid properties through the coverage of its acid sites by loading different amounts of Ni metal (5,
415 10, 12.5, and 15 wt%). The Py-IR results (Table 7) support the successful reduction in the
416 densities of Brønsted-acid sites with increasing Ni loads, and accordingly, the alkane yields were
417 projected to increase and the AHC yields to decrease. However, the phenomena observed in
418 Figure 10(b) do not agree with these conjectures. Even the AHC yield exhibits a tendency to
419 decrease, on the whole, with the increasing Ni contents. However, the highest AHC yield of 53.96
420 wt% was obtained for a Ni content of 10 wt%. Note that the olefin yields obtained with 10 and
421 12.5 wt% Ni are lower than those achieved for 5 and 15 wt% Ni, as shown in Figure 9(b).

422 In view of these results, these four catalysts were characterized in detail by XRD, SEM, and
423 TEM. The catalyst XRD patterns in Figure S5 in the SI show that Ni metal was successfully
424 loaded on the HZSM-5. The SEM and TEM results illustrated in Figure 11 reveal that the Ni

425 particle size increases with increased Ni loading. Moreover, it is interesting to note that the
 426 morphology of the loaded Ni nanoparticles exhibits polyhedral shapes for the 10 wt% Ni content,
 427 such as the tetrahedron example shown in Figure 11(b), whereas round shapes are observed for 5
 428 and 15 wt% Ni. When the Ni content is 12.5 wt%, both polyhedral and round Ni nanoparticles are
 429 evident (Figure 11(c)). Notably, more round than polyhedral particles are observed, suggesting the
 430 disappearance of the polyhedrons. Previous studies have demonstrated that the morphology of a
 431 metal catalyst substantially influences its catalytic activity^{25, 56-58}, and irregularly shaped metal
 432 centers provided abundant surface defects as active sites, which exhibit high catalytic activity^{59, 60}.
 433 Recently, Qiao and Yang^{61, 62} successfully obtained a single-atom catalyst which exhibited
 434 extremely high catalytic activity, suggesting that catalysts based on single-atom dispersions would
 435 be highly desirable to maximize atom efficiency. Based on these results, the polyhedral
 436 morphology of the Ni nanoparticles in our catalysts may expose more surface defects, and the Ni
 437 loading of 10 wt% may increase the number of accessible surface metal atoms, which would both
 438 facilitate the Diels-Alder reactions and lead to higher AHC production.



439
 440 Figure 11. Microstructural images of the prepared catalysts (Si/Al = 25): SEM images of HZSM-5
 441 with different Ni loadings: (a) 5.0, (b) 10, (c) 12.5, and (d) 15 wt%; (e) TEM and (f) HRTEM
 442 images of HZSM-5 with 10 wt% Ni loading. The loaded Ni particles showed round morphology in

443 (a), (c) and (d) whereas polyhedron morphology in (b).

444 **4 Conclusions**

445 The one-step hydroprocessing of fatty acids for the sustainable production of aromatic
446 hydrocarbons was conducted over Ni/HZSM-5 catalysts. A yield of ~64% AHCs was obtained by
447 hydroprocessing 10 g fatty acids in the presence of 0.6 g catalyst comprising 10 wt% Ni/HZSM-5
448 with a Si/Al ratio of 25 for 12 h at 360°C and 4 MPa H₂. The major reaction pathways involved in
449 the one-step transformation consisted of hydrodeoxygenation, hydrocracking, and aromatization
450 reactions. During the hydrodeoxygenation process, the unsaturated oleic and linoleic acids in the
451 feedstock were hydrosaturated to stearic acid at a low reaction temperature. Subsequently, the
452 stearic acid was transformed into the long-chain hydrocarbons octadecane and heptadecane
453 through a series of dehydration, decarbonylation, and decarboxylation reactions. Conversely,
454 unsaturated acids could be directly hydrodeoxygenated to long-chain olefins, as in the conversion
455 of oleic acid to 8-heptadecene. These pathways could be well performed on metal sites. However,
456 the hydrocracking of the long-chain hydrocarbons was performed on the catalyst acid sites rather
457 than metal sites. Through thermal and catalytic cracking reactions, the long-chain hydrocarbons
458 were transformed into gaseous products such as methane, ethane, propane, C₆–C₈ olefins, and a
459 fraction of alkanes. Subsequently, these cracked small molecules cyclized to form cyclic
460 hydrocarbons with five- or six-membered rings that could be transformed into the AHCs after
461 ring-expansion and dehydrogenation reactions. The C₆–C₈ olefins were determined to be crucial
462 intermediates for AHC formation. Lower numbers of catalytic Brønsted and Lewis acid sites
463 restricted the hydrocracking and aromatization reactions, respectively, and both led to a decrease
464 in AHC production. Additional Ni loading led to a decrease in the Brønsted acid site contents. A
465 polyhedral morphology was found for the loaded Ni nanoparticles at a Ni content of 10 wt%,
466 which may have exposed more metal defects and accessible surface metal atoms to promote AHC
467 formation. This work provides a simple, effective approach for the mass production of renewable
468 AHCs and will be helpful in utilizing such oxygenous-rich substrates in large scales for the
469 effective synthesis of renewable transportation fuels to release the atmosphere warming
470 deterioration.

471 **Acknowledgements**

472 This work was financially supported by the National Natural Science Foundation of China (No.

473 21576260), the Natural Science Foundation of Guangdong Province (No. 2016A030308004), the
474 Special Funds of Applied Science and Technology Research of Guangdong Province (No.
475 2015B020241002) and the Natural Science Foundation of Guangdong Province (No.
476 2015A030313720).

477 **References**

- 478 1. G. Liu, B. Yan and G. Chen, *Renewable and Sustainable Energy Reviews*, 2013, **25**, 59-70.
- 479 2. A. Dominguez-Ramos, B. Singh, X. Zhang, E. G. Hertwich and A. Irbien, *Journal of Cleaner*
480 *Production*, 2015, **104**, 148-155.
- 481 3. X. Zhao, L. Wei, J. Julson, Q. Qiao, A. Dubey and G. Anderson, *New Biotechnology*, 2015, **32**,
482 300-312.
- 483 4. C. Kordulis, K. Bourikas, M. Gousi, E. Kordouli and A. Lycourghiotis, *Applied Catalysis*
484 *B-Environmental*, 2016, **181**, 156-196.
- 485 5. L. Yu, S. Huang, S. Zhang, Z. Liu, W. Xin, S. Xie and L. Xu, *ACS Catalysis*, 2012, **2**, 1203-1210.
- 486 6. J. Q. Bond, A. A. Upadhye, H. Olcay, G. A. Tompsett, J. Jae, R. Xing, D. M. Alonso, D. Wang, T. Y.
487 Zhang, R. Kumar, A. Foster, S. M. Sen, C. T. Maravelias, R. Malina, S. R. H. Barrett, R. Lobo, C. E.
488 Wyman, J. A. Dumesic and G. W. Huber, *Energy & Environmental Science*, 2014, **7**, 1500-1523.
- 489 7. J. A. Melero, J. Iglesias and A. Garcia, *Energy & Environmental Science*, 2012, **5**, 7393-7420.
- 490 8. H. Olcay, A. V. Subrahmanyam, R. Xing, J. Lajoie, J. A. Dumesic and G. W. Huber, *Energy &*
491 *Environmental Science*, 2013, **6**, 205-216.
- 492 9. J. C. Serrano-Ruiz and J. A. Dumesic, *Energy & Environmental Science*, 2011, **4**, 83-99.
- 493 10. S. K. Green, R. E. Patet, N. Nikbin, C. L. Williams, C.-C. Chang, J. Yu, R. J. Gorte, S. Caratzoulas,
494 W. Fan, D. G. Vlachos and P. J. Dauenhauer, *Applied Catalysis B: Environmental*, 2016, **180**,
495 487-496.
- 496 11. T.-W. Kim, S.-Y. Kim, J.-C. Kim, Y. Kim, R. Ryoo and C.-U. Kim, *Applied Catalysis B:*
497 *Environmental*, 2016, **185**, 100-109.
- 498 12. C.-C. Chang, H. Je Cho, J. Yu, R. J. Gorte, J. Gulbinski, P. Dauenhauer and W. Fan, *Green*
499 *Chemistry*, 2016, **18**, 1368-1376.
- 500 13. Y. T. Cheng and G. W. Huber, *Green Chemistry*, 2012, **14**, 3114-3125.
- 501 14. N. Nikbin, P. T. Do, S. Caratzoulas, R. F. Lobo, P. J. Dauenhauer and D. G. Vlachos, *Journal of*
502 *Catalysis*, 2013, **297**, 35-43.
- 503 15. Y. P. Wijaya, I. Kristianto, H. Lee and J. Jae, *Fuel*, 2016, **182**, 588-596.
- 504 16. C.-C. Chang, S. K. Green, C. L. Williams, P. J. Dauenhauer and W. Fan, *Green Chemistry*, 2014,
505 **16**, 585-588.
- 506 17. M. Mohammad, T. K. Hari, Z. Yaakob, Y. C. Sharma and K. Sopian, *Renew Sust Energ Rev*, 2013,
507 **22**, 121-132.
- 508 18. A. Galadima and O. Muraza, *Journal of Industrial and Engineering Chemistry*, 2015, **29**, 12-23.
- 509 19. L. Q. Yang, K. L. Tate, J. B. Jasinski and M. A. Carreon, *ACS Catalysis*, 2015, **5**, 6497-6502.
- 510 20. B. Al Alwan, S. O. Salley and K. Y. S. Ng, *Applied Catalysis a-General*, 2015, **498**, 32-40.
- 511 21. L. G. Chen, J. Y. Fu, L. M. Yang, Z. B. Chen, Z. H. Yuan and P. M. Lv, *Chemcatchem*, 2014, **6**,
512 3482-3492.
- 513 22. L. G. Chen, H. W. Li, J. Y. Fu, C. L. Miao, P. M. Lv and Z. H. Yuan, *Catalysis Today*, 2016, **259**,
514 266-276.

- 515 23. D. Verma, R. Kumar, B. S. Rana and A. K. Sinha, *Energy & Environmental Science*, 2011, **4**,
516 1667-1671.
- 517 24. Q. Liu, H. Zuo, T. Wang, L. Ma and Q. Zhang, *Applied Catalysis A: General*, 2013, **468**, 68-74.
- 518 25. M. Tao, X. Meng, Y. Lv, Z. Bian and Z. Xin, *Fuel*, 2016, **165**, 289-297.
- 519 26. T. Li, J. Cheng, R. Huang, J. H. Zhou and K. F. Cen, *Bioresource Technology*, 2015, **197**, 289-294.
- 520 27. M. Rabaev, M. V. Landau, R. Vidruk-Nehemya, V. Koukouliev, R. Zarchin and M. Herskowitz,
521 *Fuel*, 2015, **161**, 287-294.
- 522 28. D. Jovanovic, R. Radovic, L. Mares, M. Stankovic and B. Markovic, *Catalysis Today*, 1998, **43**,
523 21-28.
- 524 29. M. Gabrovska, J. Krstić, R. Edreva-Kardjieva, M. Stanković and D. Jovanović, *Applied Catalysis*
525 *A: General*, 2006, **299**, 73-83.
- 526 30. B. X. Peng, Y. Yao, C. Zhao and J. A. Lercher, *Angewandte Chemie-International Edition*, 2012,
527 **51**, 2072-2075.
- 528 31. G. C. Li, F. Zhang, L. Chen, C. H. Zhang, H. Huang and X. B. Li, *Chemcatchem*, 2015, **7**,
529 2646-2653.
- 530 32. Y. Yang, Q. Wang, X. Zhang, L. Wang and G. Li, *Fuel Processing Technology*, 2013, **116**,
531 165-174.
- 532 33. C. Gong, H. Ning, J. Xu, Z. Li, Q. Zhu and X. Li, *Journal of Analytical and Applied Pyrolysis*, 2014,
533 **110**, 463-469.
- 534 34. T. F. Narbeshuber, H. Vinek and J. A. Lercher, *Journal of Catalysis*, 1995, **157**, 388-395.
- 535 35. S. Schallmoser, T. Ikuno, M. F. Wagenhofer, R. Kolvenbach, G. L. Haller, M. Sanchez-Sanchez
536 and J. A. Lercher, *Journal of Catalysis*, 2014, **316**, 93-102.
- 537 36. R. O. Idem, S. P. R. Katikaneni and N. N. Bakhshi, *Fuel Processing Technology*, 1997, **51**,
538 101-125.
- 539 37. S. P. R. Katikaneni, J. D. Adjaye, R. O. Idem and N. N. Bakhshi, *Industrial & Engineering*
540 *Chemistry Research*, 1996, **35**, 3332-3346.
- 541 38. V. B. Kazansky and I. N. Senchenya, *Journal of Catalysis*, 1989, **119**, 108-120.
- 542 39. V. B. Kazansky, M. V. Frash and R. A. van Santen, *Catalysis Letters*, 1994, **28**, 211-222.
- 543 40. S. Kotrel, H. Knözinger and B. C. Gates, *Microporous and Mesoporous Materials*, 2000, **35-36**,
544 11-20.
- 545 41. J. A. van Bokhoven, A. M. J. van der Eerden and R. Prins, *Journal of the American Chemical*
546 *Society*, 2004, **126**, 4506-4507.
- 547 42. A. Corma, G. W. Huber, L. Sauvanaud and P. O'Connor, *Journal of Catalysis*, 2007, **247**,
548 307-327.
- 549 43. D. Depeyre, C. Flicoteaux and C. Chardaire, *Industrial & Engineering Chemistry Process Design*
550 *and Development*, 1985, **24**, 1251-1258.
- 551 44. C. L. Williams, C. C. Chang, P. Do, N. Nikbin, S. Caratzoulas, D. G. Vlachos, R. F. Lobo, W. Fan
552 and P. J. Dauenhauer, *Acs Catalysis*, 2012, **2**, 935-939.
- 553 45. M. Vandichel, D. Lesthaeghe, J. V. d. Mynsbrugge, M. Waroquier and V. Van Speybroeck,
554 *Journal of Catalysis*, 2010, **271**, 67-78.
- 555 46. Y. V. Joshi, A. Bhan and K. T. Thomson, *The Journal of Physical Chemistry B*, 2004, **108**,
556 971-980.
- 557 47. Y. V. Joshi and K. T. Thomson, *The Journal of Physical Chemistry C*, 2008, **112**, 12825-12833.
- 558 48. H. Chen, Q. F. Wang, X. W. Zhang and L. Wang, *Applied Catalysis B-Environmental*, 2015, **166**,

- 559 327-334.
- 560 49. M. Ahmadi, A. Nambo, J. B. Jasinski, P. Ratnasamy and M. A. Carreon, *Catalysis Science &*
561 *Technology*, 2015, **5**, 380-388.
- 562 50. M. J. Mendes, O. A. A. Santos, E. Jordao and A. M. Silva, *Applied Catalysis a-General*, 2001,
563 **217**, 253-262.
- 564 51. N. Rahimi and R. Karimzadeh, *Applied Catalysis A: General*, 2011, **398**, 1-17.
- 565 52. V. Eschenbrenner-Lux, P. Kuchler, S. Ziegler, K. Kumar and H. Waldmann, *Angewandte Chemie*
566 *International Edition*, 2014, **53**, 2134-2137.
- 567 53. Y. E. Türkmen, T. J. Montavon, S. A. Kozmin and V. H. Rawal, *Journal of the American Chemical*
568 *Society*, 2012, **134**, 9062-9065.
- 569 54. H. V. Pham, R. S. Paton, A. G. Ross, S. J. Danishefsky and K. N. Houk, *Journal of the American*
570 *Chemical Society*, 2014, **136**, 2397-2403.
- 571 55. J. J. Pacheco, J. A. Labinger, A. L. Sessions and M. E. Davis, *ACS Catalysis*, 2015, **5**, 5904-5913.
- 572 56. H. Pan, B. Liu, J. Yi, C. Poh, S. Lim, J. Ding, Y. Feng, C. H. A. Huan and J. Lin, *The Journal of*
573 *Physical Chemistry B*, 2005, **109**, 3094-3098.
- 574 57. S. Zhang, Y. Hao, D. Su, V. V. T. Doan-Nguyen, Y. Wu, J. Li, S. Sun and C. B. Murray, *Journal of*
575 *the American Chemical Society*, 2014, **136**, 15921-15924.
- 576 58. S. Behtash, J. M. Lu and A. Heyden, *Catalysis Science & Technology*, 2014, **4**, 3981-3992.
- 577 59. C. Wu and P. T. Williams, *Applied Catalysis B: Environmental*, 2011, **102**, 251-259.
- 578 60. J. F. Xiang, X. Wen and F. Z. Zhang, *Industrial & Engineering Chemistry Research*, 2014, **53**,
579 15600-15610.
- 580 61. B. Qiao, A. Wang, X. Yang, L. F. Allard, Z. Jiang, Y. Cui, J. Liu, J. Li and T. Zhang, *Nat Chem*, 2011,
581 **3**, 634-641.
- 582 62. X.-F. Yang, A. Wang, B. Qiao, J. Li, J. Liu and T. Zhang, *Accounts of Chemical Research*, 2013, **46**,
583 1740-1748.
- 584
- 585